Available online at www.sciencedirect.com
ScienceDirect
Bioorganic & Medicinal Chemistry Letters
Bioorganic & Medicinal Chemistry Letters 17 (2007) 4942–4946

Experimental and theoretical study on the structure and electronic spectra of imiquimod and its synthetic intermediates

Bo Zhao,[a,*] Yu-Zhi Rong,[a] Xiao-Hua Huang[a] and Jing-Shan Shen[b,*]

[a]*College of Chemistry and Environmental Science, Nanjing Normal University, Nanjing 210097, PR China*
[b]*Shanghai Institute of Materia Medica, SIBS, Chinese Academy of Sciences, 555, Zuchongzhi Road, Zhangjiang High-Tech Park, Shanghai 201203, China*

Received 25 April 2007; revised 2 June 2007; accepted 7 June 2007
Available online 10 June 2007

Abstract—Crystal structure of the imiquimod has been determined by single crystal X-ray analysis, imiquimod crystallizes in orthorhombic space group $P2_12_12_1$ and the molecules are linked along the c axis by the strong N–H···N hydrogen bonds. A density functional theory (DFT) study on the electronic properties of imiquimod and its synthetic intermediates has been performed at B3LYP/6-31G* level, while taking solvent effects into account. Both the single configuration interaction (CIS) method and the time-dependent DFT (TDDFT) approaches have been used to calculate the electronic absorption spectra, and there is a good agreement between the calculated and experimental UV–visible absorption spectra. The fluorescence emission spectra of these three compounds in solution have also been measured, the relatively low fluorescence intensity is attributed to a chlorine-modulated heavy atom effect that enhances intersystem crossing between excited singlet and triplet states, and the relatively high fluorescence intensity of imiquimod results from an extended π-conjugated system which enhances $S_1 \rightarrow S_0$ radiant transition.

Since the discovery of interferon (IFN) and its potential for the treatment of viral infections and cancer, there have been increasing studies for small-molecule inducers of this cytokine. A number of compounds that induce IFN in mice have been identified, but few are active in human cells.[1] While working on potential antiherpes agents, a series of 1*H*-imidazo[4,5-*c*]quinolines that induce IFN in mice, guinea pigs, monkeys, and humans were discovered,[2–4] studies on which have led to the development of imiquimod (1-(2-methylpropyl)-1*H*-imidazo[4,5-*c*]quinoline-4-amine), for clinical use. Imiquimod had the right balance of activity and tolerability for the prevention of lesions caused by herpes simplex virus-2 (HSV-2) infection in the guinea pig model.[5] The observed antiviral activity in vivo is associated with the production of IFN in a cell-mediated immune response. It has been demonstrated that topical application of imiquimod in humans induces synthesis of IFN and other cytokines in skin at the application site.[3] Clinical utility has been demonstrated in treating genital warts, basal cell carcinoma, and actinic keratosis.[6–11] This novel series of immune response modifiers will still need to be explored in order to find small molecules that treat diseases involving the immune system.[12,13]

Imiquimod as well as synthetic intermediates: 1-(2-methylpropyl)-1*H*-imidazo[4,5-*c*]quinoline and 4-chloro-1-(2-methylpropyl)-1*H*-imidazo[4,5-*c*]quinoline have been plentifully synthesized and extensively experimented in vitro and in vivo as potential antiviral agents, but their crystal structure, electronic properties, electronic and fluorescence spectra have never been studied. In this paper, we performed experimental studies on electronic, fluorescence spectra properties and theoretical studies on the above-mentioned properties which have vital significance in the future study and hope that our data can help the chemists in finding some indications for the future use in medical applications of imidazoquinoline compounds.

Molecular structures of the title compounds are depicted in Figure 1 (II). All compounds have been fully optimized at the B3LYP (DFT) level with the 6-31G* basis set and characterized by the calculations of vibrational frequencies at the same level. The effects of solvent on electronic structures have been simulated by an Onsager

Keywords: Imiquimod; Density functional theory; Electronic absorption spectra; Fluorescence emission spectra.
* Corresponding authors. Tel.: +86 25 83598053 (B.Z.); e-mail addresses: zhaobo@njnu.edu.cn; dr-zhaobo@hotmail.com

0960-894X/$ - see front matter © 2007 Elsevier Ltd. All rights reserved.
doi:10.1016/j.bmcl.2007.06.020

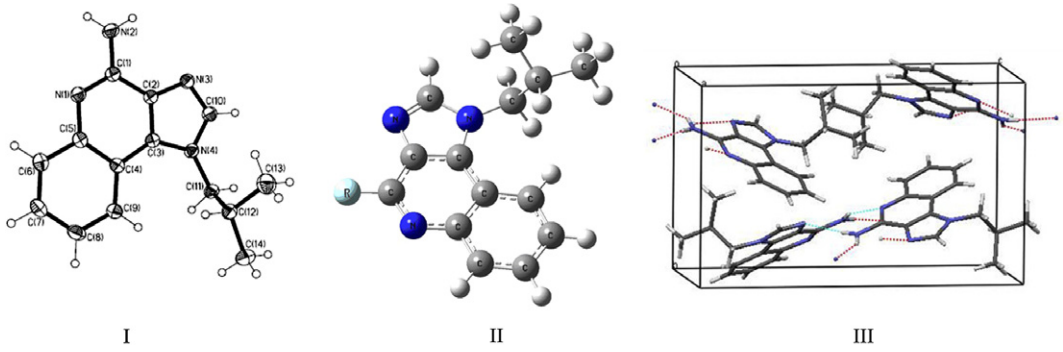

I II III

Figure 1. Structure of the imiquimod with atomic numbering (I); molecular structures of the organic compounds studied in this work (II) for a (R = H), b (R = Cl), and c (R = NH_2); the intermolecular hydrogen bonds in the crystal structure of imiquimod (III).

model with solvent parameters performed using SCRF/dipole scheme. The Onsager reaction field model[14–19] places the solute in a fixed spherical cavity of radius a_0 within the solvent field. We have selected water to research the solvent effects on them. The values of cavity size (a_0) are 4.87 Å, 5.19 Å, and 5.04 Å for a, b, and c, respectively, and the dielectric constant of water is the default value. The electronic absorption spectra have also been calculated using two different methods: the single configuration interaction (CIS)[20,21] and the time-dependent DFT (TDDFT),[22–25] both basing on the B3LYP/6-31G* level optimized structures. In order to better compare theoretical and experimental absorption spectra, we assume the Gaussian band width the same as the experimental absorption spectra. A line spectrum is directly obtained by the output file of Gaussian and we use a Swizard file to draw the spectrum by the Origin software. The Mulliken atomic charges for partial selected atoms of the three compounds in gas and in water are listed in Table 4. All theoretical calculations are carried out using GAUSSIAN 03 suite of programs[26] and using the default convergence criteria.

The imiquimod single crystal has been selected for data collection at 273(2) K, using a CCD area detector with graphite monochromated Mo K_α radiation (λ = 0.71073 Å). The data have been collected by ω scan technique and the structure has been solved by direct methods using SHELXL-97 program package.[27] Crystal data and structure refinement parameters are listed in Table 1. The molecular structure with atomic numbering scheme of the imiquimod is shown in Figure 1 (I). The intermolecular hydrogen bonds are shown in Figure 1 (III). Table 2 lists its bond lengths, angles, and symmetry code. Crystallographic data (excluding structure factors) for the structures in this paper have been deposited with the Cambridge Crystallographic Data Centre as supplementary publication numbers CCDC 637851. The selected experimental and optimized geometric parameters as bond lengths and torsion angles are listed in Table 3.

The imiquimod crystallizes in orthorhombic crystal system and forms noncentrosymmetric space group $P2_12_12_1$. In the unit cell the molecules are head-to-head linked along the c axis by the strong N–H···N hydrogen bonds between the amino group and imidazole ring

Table 1. Crystallographic data and structure refinement parameters of the imiquimod

	Compound c (imiquimod)
Empirical formula	$C_{14}H_{16}N_4$
Crystal system	Orthorhombic
Space group	$P2_12_12_1$
Unit cell parameters	
a (Å)	8.1327(6)
b (Å)	9.7473(6)
c (Å)	15.7524(10)
β (°)	90
V (Å^3)	1248.72(14)
Z	4
D (Mg/m^3)	1.278
Absorption coefficient (mm^{-1})	0.080
F(000)	512
Final R_1 and wR_2 [$I > 2\sigma(I)$]	0.0384, 0.0767
R_1 and wR_2 indices (all data)	0.0502, 0.0811
Largest diff. peak and hole (e/Å^{-3})	0.123 and −0.195

Table 2. Intermolecular hydrogen bonds in the imiquimod crystal

D–H···A	d(D–H)	d(H···A)	d(D···A)	∠(DHA)
N2–H (2A)···N3[a]	0.86	2.24	3.1011(16)	175.5
N2–H (2B)···N1[b]	0.86	2.33	3.1265(16)	153.6

Symmetry transformations used to generate equivalent atoms: [a] $x - 1/2, -y + 3/2, -z + 1$. [b] $x + 1/2, -y + 3/2, -z + 1$.

(Table 2), which contribute to the high thermal stability (mp 292–294 °C). As can be seen from Table 3, the bond lengths of the C–C and C–N in imidazoquinoline ring are shorter than their natural single bond lengths, suggesting that the C–C and C–N bonds in imidazoquinoline ring have part double bond character, among which the bond lengths of C1–N1, C6–C7, C8–C9, and C10–N3 are relatively shorter. The crystal structure data indicate that the imidazole, benzene, pyridine, and the connected amino group are coplanar in the whole molecule (the torsion angles of N1–C5–C4–C9, C1–C2–C3–N4, and N2–C1–C2–C3 are nearly 180°). The optimized geometric parameters in Table 3 are in good agreement with the X-ray experimental results.

Seen from the calculated results for a and b in Table 4, the nitrogen atoms have relatively big negative atomic charges, especially the atom N1 on the quinoline ring

Table 3. Selected experimental and optimized geometric parameters of the imiquimod

Parameters	X-ray analysis	B3LYP/6-31G*
The bond lengths (Å)		
C1–N2	1.3533(18)	1.3691
C1–C2	1.4239(19)	1.4297
C2–C3	1.3775(18)	1.3937
C3–C4	1.4263(19)	1.4320
C4–C5	1.4218(19)	1.4400
C5–N1	1.3847(17)	1.3736
C1–N1	1.3201(17)	1.3170
C5–C6	1.410(2)	1.4163
C6–C7	1.367(2)	1.3809
C7–C8	1.390(2)	1.4081
C8–C9	1.371(2)	1.3831
C4–C9	1.4115(19)	1.4142
C2–N3	1.3892(17)	1.3792
C3–N4	1.3855(18)	1.3886
C10–N3	1.3064(18)	1.3101
C10–N4	1.3669(19)	1.3794
The torsion angles (°)		
N1–C5–C4–C9	−178.61(13)	−179.51
C1–C2–C3–N4	178.74(12)	−179.92
N2–C1–C2–C3	−179.29(13)	−177.54

acts as the electronegative potential site of the whole molecule and the atom C3 has the biggest positive atomic charges. It can be found that the atomic charge values of atoms N1 and C3 in solution-phase are bigger than those in gas-phase. Atom C1, whose atomic charge value increases dramatically when the hydrogen atom is substituted by the amino-group, turns to the electropositive potential site, and the nitrogen atom of the substituted amino-group turns to the electronegative potential site of the imiquimod. Moreover, their atomic charge values in solution-phase are smaller than those in gas-phase. The main route for charge transfer of the whole molecule has changed from N1 → C3 to N2 → C1. The atomic charge values of atoms C3 and N1 in solution-phase also increase comparing that in gas-phase.

We have calculated the electronic absorption spectra using both the CIS method at *cis*/6-31G* and the TD-DFT method at B3LYP/6-31G* levels based on the optimized structures and twenty bands of electronic transition are selected. The experimental and calculated maximum absorption wavelengths (λ_{max}) and corresponding oscillator strengths (f) of the three compounds are reported in Table 5.

Figure 2 presents experimental UV–visible absorption spectra of a, b and c in water solution containing 20% methanol. We find that the presence of chlorine atom at the 1-position results in no major perturbation of UV–visible absorption λ_{max}, while λ_{max} of c is red-shifted in comparison with a and b as the result of an extended π-conjugated system when the substitute of amino-group at the 1-position, which reduces the energy differences between the ground state and the excited states.

The calculated UV–visible absorption spectra are also shown in Figure 2. The calculated values of molar absorptivity are plotted versus the wavelength included in CIS and TDDFT calculations. The TDDFT method gives slightly underestimated values, while the SCI method underestimates λ_{max} by about 50 nm for the three compounds. The calculated λ_{max} follows the trend λ_{max} (c) > λ_{max} (b) > λ_{max} (a), in good agreement with the experimental data. The experimental values of f are situated between the values calculated by TDDFT and CIS. The above results indicate that the overall performance of the TDDFT method is better than the CIS approach for the three organic compounds. There is a certain extent deviation between calculated results and experimental data as our calculated results are obtained in the molecular level, while actual values are related to concrete experimental condition.

Figure 3 presents fluorescence emission spectra of a, b, and c in water solution containing 20% methanol. The fluorescence emission λ_{max} of c is red-shifted with respect to a and b (341 nm for a, 343 nm for b, and 351 nm for c), as is also expected from an extended π-conjugated system when the substitute of amino-group is at the 1-position, which reduces the energy

Table 4. The Mulliken atomic charges for partial selected atoms calculated in gas-phase and in solution-phase (water, $\varepsilon = 78.39$)

Atoms	Compound a (R′ = H)		Compound b (R′ = Cl)		Compound c (R′ = N)	
	Gas	Water	Gas	Water	Gas	Water
N1	−0.518	−0.530	−0.519	−0.529	−0.631	−0.636
N3	−0.502	−0.514	−0.484	−0.498	−0.529	−0.534
N4	−0.508	−0.507	−0.509	−0.507	−0.517	−0.516
C1	0.019	0.013	0.066	0.067	0.478	0.464
C2	0.185	0.186	0.211	0.214	0.156	0.158
C3	0.269	0.274	0.279	0.283	0.285	0.290
C4	0.156	0.154	0.167	0.166	0.147	0.145
C5	0.224	0.225	0.214	0.213	0.239	0.239
C6	−0.144	−0.146	−0.144	−0.145	−0.162	−0.163
C7	−0.134	−0.133	−0.134	−0.132	−0.131	−0.131
C8	−0.141	−0.142	−0.140	−0.140	−0.149	−0.150
C9	−0.196	−0.194	−0.197	−0.195	−0.198	−0.196
C10	0.207	0.209	0.211	0.213	0.210	0.212
R′[a]	0.151	0.129	0.015	−0.032	−0.774	−0.773

R′ is H atom, Cl atom, and N atom for a, b, and c, respectively.

Table 5. Calculated and experimental maximum absorption wavelengths (λ_{max}) and oscillator strengths (f)

Compound	TDDFT		CIS		Expt	
	λ_{max} (nm)	f	λ_{max} (nm)	f	λ_{max} (nm)	f[a]
a	226.2	0.692	180.5	1.783	235	1.546
b	230.0	0.805	181.5	1.879	238	1.658
c	232.6	0.669	182.9	1.636	245	1.041

ε_m, maximum molar absorptivity (M^{-1} cm^{-1}); υ, wavenumber (cm^{-1}); $\Delta\upsilon_{1/2}$, width at half-height (cm^{-1}).
[a] Experimental f is given as follows. $f = 4.32 \times 10^{-9} \int \varepsilon_m \, d\upsilon \approx 4.32 \times 10^{-9} \times 1.0645 \varepsilon_{max} \Delta\upsilon_{1/2}$.

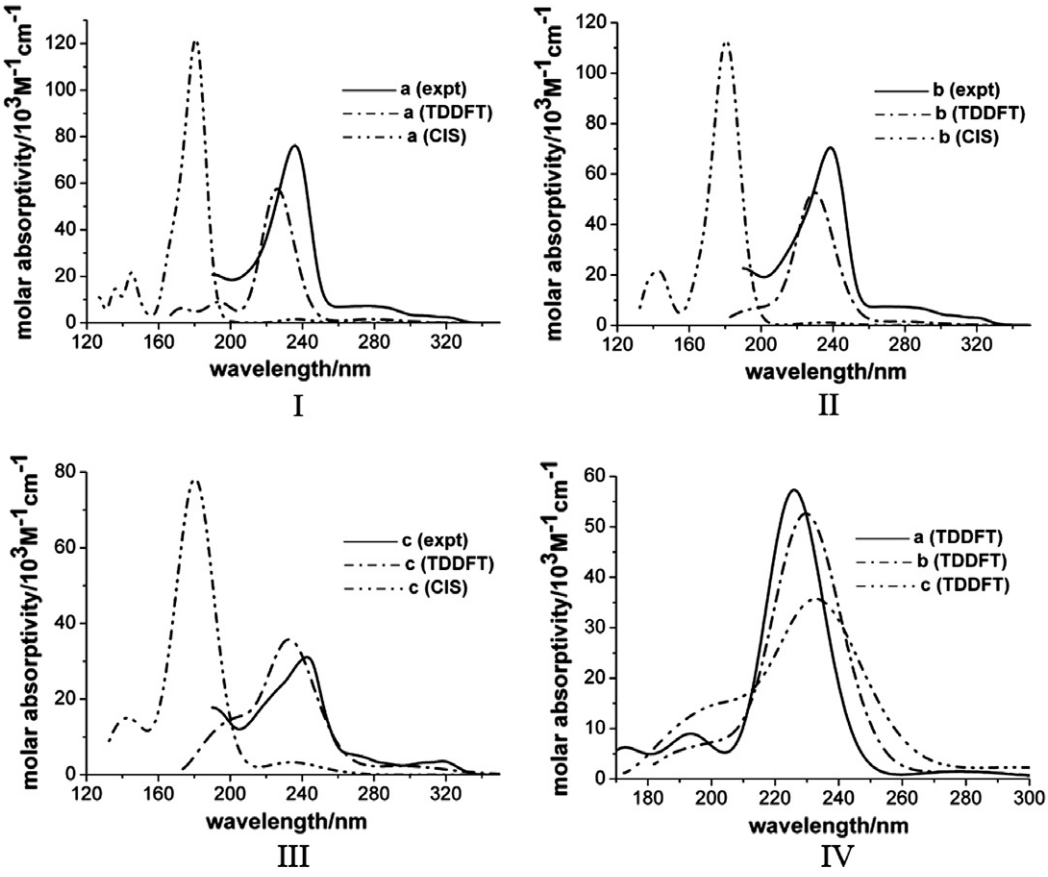

Figure 2. Simulated UV–visible absorption spectra calculated at CIS/6-31G* and TD-B3LYP/6-31G* levels, experimental UV–visible absorption spectra measured in water solution containing 20% methanol of 0.02 mM a, b, and c.

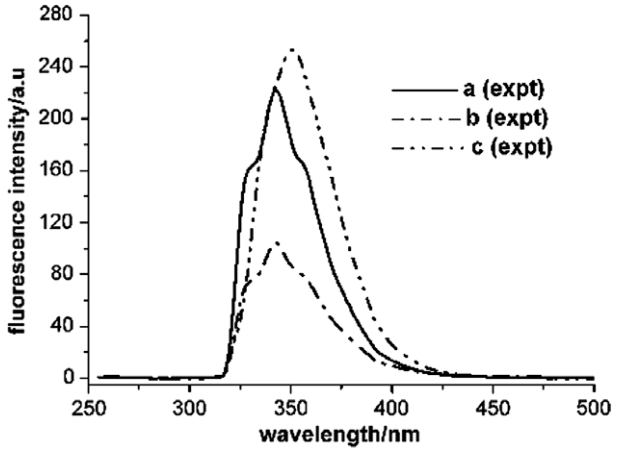

Figure 3. Fluorescence emission spectra measured in water solution containing 20% methanol of 0.02 mM a, b, and c. For a and b, excitation and emission slits are all 5 nm; for c, excitation and emission slits are all 2.5 nm.

differences between the first singlet-spin excited state and singlet-spin ground state. The fluorescence intensity (I_f) follows the trend I_f (c) > I_f (a) > I_f (b). The relatively low I_f of b is attributed to the presence of chlorine atom at the 9-position, which increases the lowest triplet (T_1) populations by enhancing $S_0 \rightarrow T_1$ absorption transition and $S_1 \rightarrow T_1$ intersystem crossing. The fluorescence intensity of c is much higher than that of a and b due to an extended π-conjugated system which enhances $S_1 \rightarrow S_0$ radiant transition when electron donating amino-group is present at the 9-position.

In the present study, we have reported crystal structure of the imiquimod. Theoretical calculations have been performed on the electronic structures and the electronic absorption spectra of the title compounds. Also, we have measured the fluorescence emission spectra and UV–visible absorption spectra of them in solution. First, imiquimod crystallizes in orthorhombic space group $P2_12_12_1$. The intermolecular hydrogen

bonds locate among the amino-group of one molecule and the imidazole rings of the other two molecules. The optimized geometric parameters are in good agreement with the experimental values. Second, the atomic charge value of the nitrogen atom on the quinoline ring which acts as the electronegative potential site of the compounds a and b increases when considering solvent effects. But the nitrogen atom of the substituted amino-group turns to the electronegative potential site of the whole imiquimod molecule and its atomic charge value decreases when considering solvent effects. Third, the λ_{max} values calculated by the CIS approach are underestimated significantly compared with the experimental values, but the TDDFT method is more suitable in general to estimate electronic absorption spectra properties of these compounds. The relatively low I_f is attributed to heavy atom effect that enhances intersystem crossing between excited singlet and triplet states, and the relatively high I_f is attributed to substituting group effect with an extended π-conjugated system that enhances $S_1 \rightarrow S_0$ radiant transition.

Acknowledgments

We are grateful for funding from the Nature Science Foundation of Jiangsu Province Education Ministry (05KJB430058), the Nature Science Foundation of China (20471030, 30570323), the Nature Science Foundation of Jiangsu Science and Technology Department (BK2005118).

References and notes

1. Weirenga, W. *Annu. Rep. Med. Chem.* **1982**, *18*, 151.
2. Gerster, J. F.; Lindstrom, K. J.; Miller, R. L.; Tomai, M. A.; Birmachu, W.; Bomersine, S. J.; Gibson, S. N.; Imbertson, L. M.; Jacobson, J. R.; Knafla, R. T.; Maye, P. V.; Nikolaides, N.; Oneyemi, F. Y.; Parkhurst, G. J.; Pecore, S. E.; Reiter, M. J.; Scribner, L. S.; Testerman, T. L.; Thompson, N. J.; Wagner, T. L.; Weeks, C. E.; Andre, J.-D.; Lagain, D.; Bastard, Y.; Lupu, M. *J. Med. Chem.* **2005**, *48*, 3481.
3. Miller, R. L.; Gerster, J. F.; Owens, M. L.; Slade, H. B.; Tomai, M. A. *Int. J. Immunopharmacol.* **1999**, *21*, 1.
4. Arany, I.; Tyring, S. K.; Stanley, M. A.; Tomai, M. A.; Miller, R. L.; Smith, M. H.; McDermott, D. J.; Slade, H. B. *Antiviral Res.* **1999**, *43*, 53.
5. Miller, R. L.; Imbertson, L. M.; Reiter, M. J.; Gerster, J. F. *Antiviral Res.* **1999**, *44*, 31.
6. Slade, H. B.; Owens, M. L.; Tomai, M. A.; Miller, R. L. *Expert. Opin. Invest. Drugs* **1998**, *7*, 437.
7. Edwards, L.; Ferenczy, A.; Eron, L.; Baker, D.; Owens, M. L.; Fox, T. L.; Hougham, A. J.; Schmitt, K. A.HPV Study Group *Arch. Dermatol.* **1998**, *134*, 25.
8. Marks, R.; Gebauer, K.; Shumack, S.; Amies, M.; Bryden, J.; Fox, T. L.; Owens, M. L. *J. Am. Acad. Dermatol.* **2001**, *44*, 807.
9. Geisse, J.; Caro, I.; Lindholm, J.; Golitz, L.; Stampone, P.; Owens, M. *J. Am. Acad. Dermatol.* **2004**, *50*, 722.
10. Stockfleth, E.; Meyer, T.; Benninghoff, B.; Salasche, S.; Papadopoulos, L.; Ulrich, C.; Christophers, E. *Arch. Dermatol.* **2002**, *138*, 1498.
11. Lebwohl, M.; Dinehart, S.; Whiting, D.; Lee, P. K.; Tawfik, N.; Jorizzo, J.; Lee, J. H.; Fox, T. L. *J. Am. Acad. Dermatol.* **2004**, *50*, 714.
12. Hirota, K.; Kazaoka, K.; Niimoto, I.; Kumihara, H.; Sajiki, H.; Isobe, Y.; Takaku, H.; Tobe, M.; Ogita, H.; Ogino, T.; Ichii, S.; Kurimoto, A.; Kawakami, H. *J. Med. Chem.* **2002**, *45*, 5419.
13. Kurimoto, A.; Ogino, T.; Ichii, S.; Isobe, Y.; Tobe, M.; Ogita, H.; Takaku, H.; Sajiki, H.; Hirota, K.; Kawakami, H. *Bioorg. Med. Chem.* **2004**, *12*, 1091.
14. Kirkwood, J. G. *J. Chem. Phys.* **1934**, *2*, 351.
15. Onsager, L. *J. Am. Chem. Soc.* **1936**, *58*, 1486.
16. Wong, M. W.; Frisch, M. J.; Wiberg, K. B. *J. Am. Chem. Soc.* **1991**, *113*, 4776.
17. Wong, M. W.; Wiberg, K. B.; Frisch, M. J. *J. Am. Chem. Soc.* **1992**, *114*, 523.
18. Wong, M. W.; Wiberg, K. B.; Frisch, M. J. *J. Am. Chem. Soc.* **1992**, *114*, 1645.
19. Wong, M. W.; Wiberg, K. B.; Frisch, M. J. *J. Chem. Phys.* **1991**, *95*, 8991.
20. Orr, B. J.; Ward, J. F. *Mol. Phys.* **1970**, *20*, 513.
21. Foresman, J. B.; Head-Gordon, M.; Pople, J. A.; Frisch, M. J. *J. Phys. Chem.* **1992**, *96*, 135.
22. Runge, E.; Gross, E. K. U. *Phys. Rev. Lett.* **1984**, *52*, 997.
23. Petersilka, M.; Gossmann, U. J.; Gross, E. K. U. *Phys. Rev. Lett.* **1966**, *76*, 1212.
24. Bauernschmitt, R.; Ahlrichs, R. *Chem. Phys. Lett.* **1996**, *256*, 1996.
25. Jamorski, C.; Casida, M. E.; Salahub, D. R. *J. Chem. Phys.* **1996**, *104*, 5134.
26. Frisch, M.J.; Trucks, G.W.; Schlegel, H.B.; Scuseria, G.E.; Robb, M.A.; Cheeseman, J.R.; Montgomery, J.A.; Vreven, T.; Kudin, K.N.; Burant, J.C.; Millam, J.M.; Iyengar, S.S.; Tomasi, J.; Barone, V.; Mennucci, B.; Cossi, M.; Scalmani, G.; Rega, N.; Petersson, G.A.; Nakatsuji, H.; Hada, M.; Ehara, M.; Toyota, K.; Fukuda, R.; Hasegawa, J.; Ishida, M.; Nakajima, T.; Honda, Y.; Kitao, O.; Nakai, H.; Klene, M.; Li, X.; Knox, J.E.; Hratchian, H.P.; Cross, J.B.; Adamo, C.; Jaramillo, J.; Gomperts, R.; Stratmann, R.E.; Yazyev, O.; Austin, A.J.; Cammi, R.; Pomelli, C.; Ochterski, J.W.; Ayala, P.Y.; Morokuma, K.; Voth, G.A.; Salvador, P.; Dannenberg, J.J.; Zakrzewski, V.G.; Dapprich, S.; Daniels, A.D.; Strain, M.C.; Farkas, O.; Malick, D.K.; Rabuck, A.D.; Raghavachari, K.; Foresman, J.B.; Ortiz, J.V.; Cui, Q.; Baboul, A.G.; Clifford, S.; Cioslowski, J.; Stefanov, B.B.; Liu, G.; Liashenko, A.; Piskorz, P.; Komaromi, I.; Martin, R.L.; Fox, D.J.; Keith, T.; Al-Laham, M.A.; Peng, C.Y.; Nanayakkara, A.; Challacombe, M.; Gill, P.M.W.; Johnson, B.; Chen, W.; Wong, M.W., Gonzalez, C.; Pople, J.A. Gaussian 03, Revision B.05.; Gaussian, Inc.: Pittsburgh, PA, 2003.
27. Sheldrick, G.M. SHELX97 and SHELXL97, University of Gottingen, Germany, 1997.